Nano Res
DOI 10.1007/s12274-012-0269-3
Research Article

ISSN 1998-0124
CN 11-5974/O4

Strain-Induced D Band Observed in Carbon Nanotubes

Chia-Chi Chang[1], Chun-Chung Chen[2], Wei-Hsuan Hung[3], I-Kai Hsu[4], Marcos A. Pimenta[5], and Stephen B. Cronin[1,2] (✉)

[1] Department of Physics, [2] Department of Electrical Engineering, and [4] Department of Materials Science, University of Southern California, Los Angeles, CA 90089, USA
[3] Department of Materials Science and Engineering, Feng Chia University
[5] Departamento de Física, Universidade Federal de Minas Gerais, Belo Horizonte, MG 30123-970, Brazil

Received: 27 August 2012 / Revised: 2 October 2012 / Accepted: 11 October 2012

ABSTRACT

We report the emergence of the D band Raman mode in single-walled carbon nanotubes under large axial strain. The D to G mode Raman intensity ratio (I_D/I_G) is observed to increase with strain quadratically by more than a factor of 100-fold. Up to 5% strain, all changes in the Raman spectra are reversible. The emergence of the D band, instead, arises from the reversible and elastic symmetry-lowering of the sp^2 bonds structure. Beyond 5%, we observe irreversible changes in the Raman spectra due to slippage of the nanotube from the underlying substrate, however, the D band intensity resumes its original pre-strain intensity, indicating that no permanent defects are formed.

KEYWORDS

SWCNTs, Raman, D band, defects, strain, sp^2 bond

The mechanical properties of carbon nanotubes (CNTs) have intrigued many scientists and engineers, inspiring potential applications ranging from atomic-scale mass sensors [1, 2] to space elevators [3, 4]. While being harder than diamond in their axial direction, CNTs also have an enormous elasticity, and can be strained by more than 17.5% without creating any permanent defects in the lattice, resulting in a breaking stress of 200GPa and a record high strength to weight ratio of 1.75×10^8 N·m/kg [5, 6]. Theoretical studies have predicted the breaking strain of CNTs to lie in the range from 14.5 to 22%, depending on the chiral angle, which suggests that the ultimate breaking strain of CNTs has not yet been reached [7, 8].

Unlike the more commonly studied G band and radial breathing mode, the D band Raman mode involves phonons with finite momentum [9]. Because photons carry little momentum, the D band is observed only when the momentum conservation requirement of the optical Raman process is broken by defects and disorder. Hence, the relative intensity of the D band gives a measure of the amount of disorder in the nanotube. As such, the relative intensity of the so-called defect-induced D band has been used as an indication of the quality of carbon nanotubes for many years [10–12]. More recently, the D to G mode Raman intensity ratio (I_D/I_G) in graphene has been used to determine the defect densityσ, by the relation: $\sigma\,(\mathrm{cm}^{-2}) = (1.8 \pm 0.5)\cdot\lambda^{-4}\cdot(I_D/I_G) \times 10^{22}$, where λ is the excitation wavelength in nanometers [13, 14]. However,

Address correspondence to scronin@usc.edu

no such correlation exists for CNTs. Furthermore, we expect different types of defects to affect the D band intensity differently. In a previous study, an atomic force microscope (AFM) tip was used to induce strains ranging from 0.06% to 1.65% in CNTs clamped at both ends by metal electrodes [15]. However, no general trend in the I_D/I_G Raman intensity ratio was observed. Several other prior studies have investigated the Raman spectra of carbon nanotubes under strain, none of which have reported a consistent change in the D band intensity due to strain [16–19].

In the work presented here, we investigate the D band Raman intensity using two experimental approaches to apply large strains to carbon nanotubes in a continuous, reversible fashion. In the first approach, single-walled CNTs are grown suspended across a gap separating two adjacent silicon substrates. Strain is then induced by increasing the separation between the two substrates using a micromechanical translation stage, as shown in Fig. 1(a) [5]. In the second approach, CNTs are grown on an oxidized silicon substrate and then transferred to an elastic polydimethylsiloxane (PDMS) substrate. Nearly 100% transfer of nanotubes can be achieved by first treating the PDMS substrate with an oxygen plasma. The two ends of the PDMS substrate are then mounted on a translation stage, in order to induce strain [20]. Ultra-long CNTs were grown by chemical vapor deposition using a ferric nitrate $Fe(NO_3)_3$ catalyst with H_2:CH_4:C_2H_4 at rates of 1500:1500:50 standard cubic centimeters per minute (sccm) at 900 °C for 25 minutes in a quartz tube with a 22 mm inner diameter. The ultra-long nature of these nanotubes enables the application of high strains because the total van der Waals force that can be applied depends on the length of the CNT-substrate contact (10 pN/μm) [21]. Nanotubes grown in this fashion are aligned along the direction of the gas flow. Figures 1(c) and 1(d) show scanning electron microscope (SEM) and AFM images of the suspended and PDMS samples, respectively. Bundles are typically seen in both suspended and on-substrate samples, ranging from 2–5 nm in diameter. A 532 nm laser (100 μW) was focused through a 100 × high numerical aperture objective lens (NA = 0.9) and used to collect Raman spectra from the nanotubes under strain for both samples.

Figure 2(a) shows the Raman spectra of an ultra-long suspended CNT bundle with a single resonant nanotube spanning an 82 μm wide gap. At 0% strain there are two prominent peaks corresponding to G_+ and G_- bands and an almost undetectable D band. The strain dependence of the D, G_-, and G_+ band frequencies are plotted in Figs. 2(b), 2(c), and 2(d), which exhibit downshifts of 23, 40, and 43 cm^{-1} under 5% strain, respectively. All peaks in these spectra downshift linearly and reversibly with applied strain up to 5%, indicating that no slippage occurs between the CNT bundle and the underlying substrate. The broad G_- band peak at 1577 cm^{-1} exhibits a Breit–Wigner–Fano (BWF) lineshape, typical of metallic nanotubes, which becomes more narrow under strain due to the opening of a bandgap. Strain-induced bandgaps can be created in SWCNTs under axial strain at a rate of 0 to 30 meV/% strain, depending on the chiral angle [22]. These changes in the linewidth of the G_- band are also reversible with strain, as shown in the inset of Fig. 2(c), in agreement with previous observations in metallic SWCNTs [20]. The raw spectra in Fig. 2(a) show that the D band not only downshifts but also grows in intensity as the strain increases.

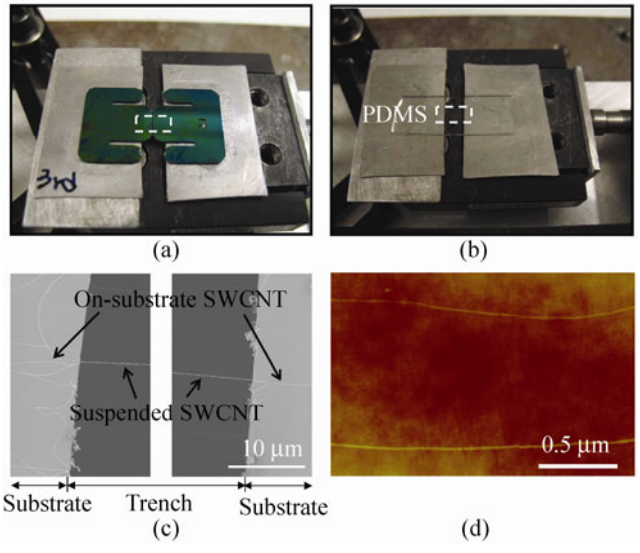

Figure 1 Photographs of the experimental setups for applying strain to (a) suspended and (b) on-substrate SWCNTs. (c) SEM images of an ultra-long suspended SWCNT spanning a 82 μm-wide gap. (d) AFM image of SWCNTs on a PDMS substrate

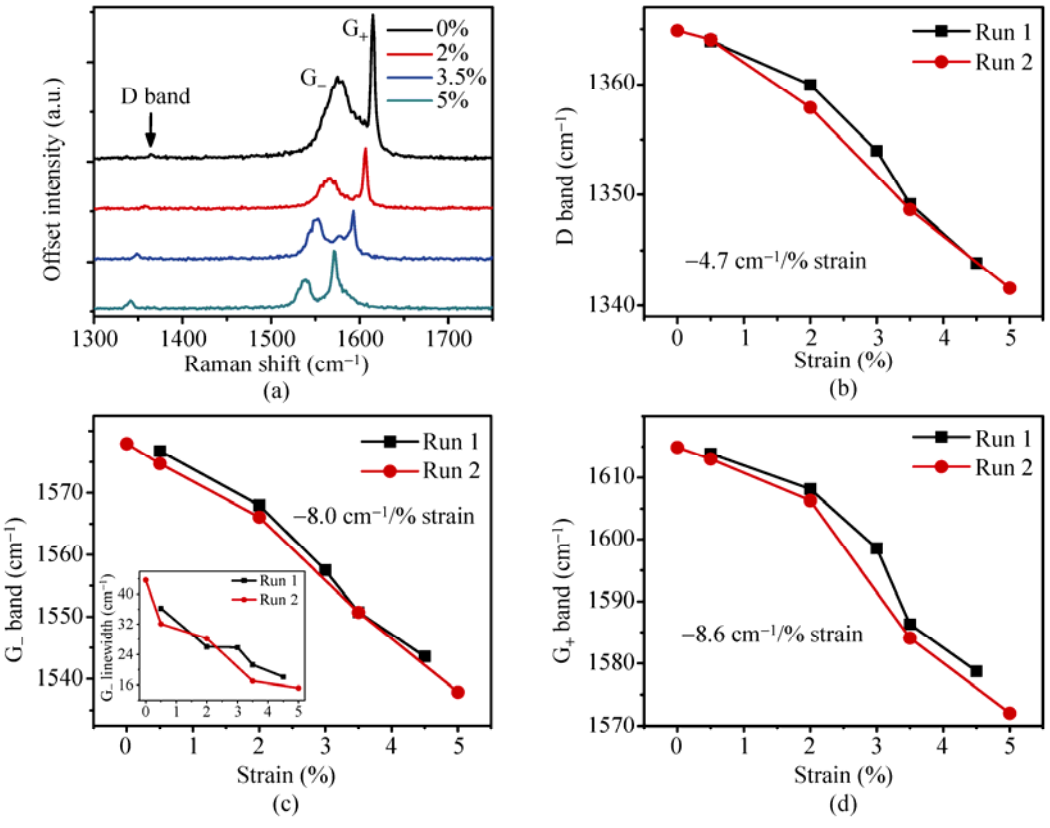

Figure 2 (a) Raman spectra of suspended carbon nanotubes at strains of 0, 2, 3.5, and 5%. (b)–(d) D, G_-, and G_+ band frequencies plotted as a function of applied strain. In run1, strain is decreased from 4.5% to 0.5%. In run 2, strain is increased from 0% to 5%

Figure 3(a) shows the D band frequency plotted as a function of the G_- band frequency. The co-linearity of this data indicates that the G_- and D bands originate from the same nanotube. The same co-linearity is observed between the G_+ and D bands (not shown here). Figure 3(b) shows the D band intensity normalized by the G band intensity plotted as a function of strain. This Raman intensity ratio (I_D/I_G) exhibits a quadratic dependence on the applied strain, and changes reversibly from 0.004 to 0.043. Since the G band downshift is expected to have a linear dependence on the C–C bond length, we plot I_D/I_G as a function of the square of the G_- band shift ($\Delta\omega_{G_-}{}^2$), and obtain the linear fit shown in Fig. 3 (c). The quadratic dependence of I_D/I_G on strain is likely due to two effects. First, there is a strain-induced reduction of the G band Raman intensity as the nanotube inter-band transition (E_{11}^M) is shifted off resonance from the laser energy inversely proportional to $\Delta\omega_{G_-}$, as shown in Fig. 3(d). Second, there is an increase of the D band intensity proportional to $\Delta\omega_{G_-}$ due to the strain-induced lowering of the symmetry, as shown in Fig. 3(e). The G band Raman intensity depends on the optical transition energy (E_{ii}) and on the laser excitation energy according to the resonance Raman process [17, 23]. With a fixed laser energy, the resonance Raman formula can be approximated to first order by a linear or an inverse linear relationship, depending on whether E_{ii} is moving toward or away from resonance. Strain-induced variations of the optical transition energies in carbon nanotubes have been studied theoretically and experimentally, showing linear dependences on the value of uniaxial strain [22, 24]. In the particular region we observed here, the G band intensity is inversely proportional to the applied strain.

In carbon nanotubes, the D band is not actually a Raman active phonon mode. However, this phonon mode can be seen in nanotubes with a large amount of disorder and defects, which break the symmetry of the lattice and relax the selection rules. Large amounts

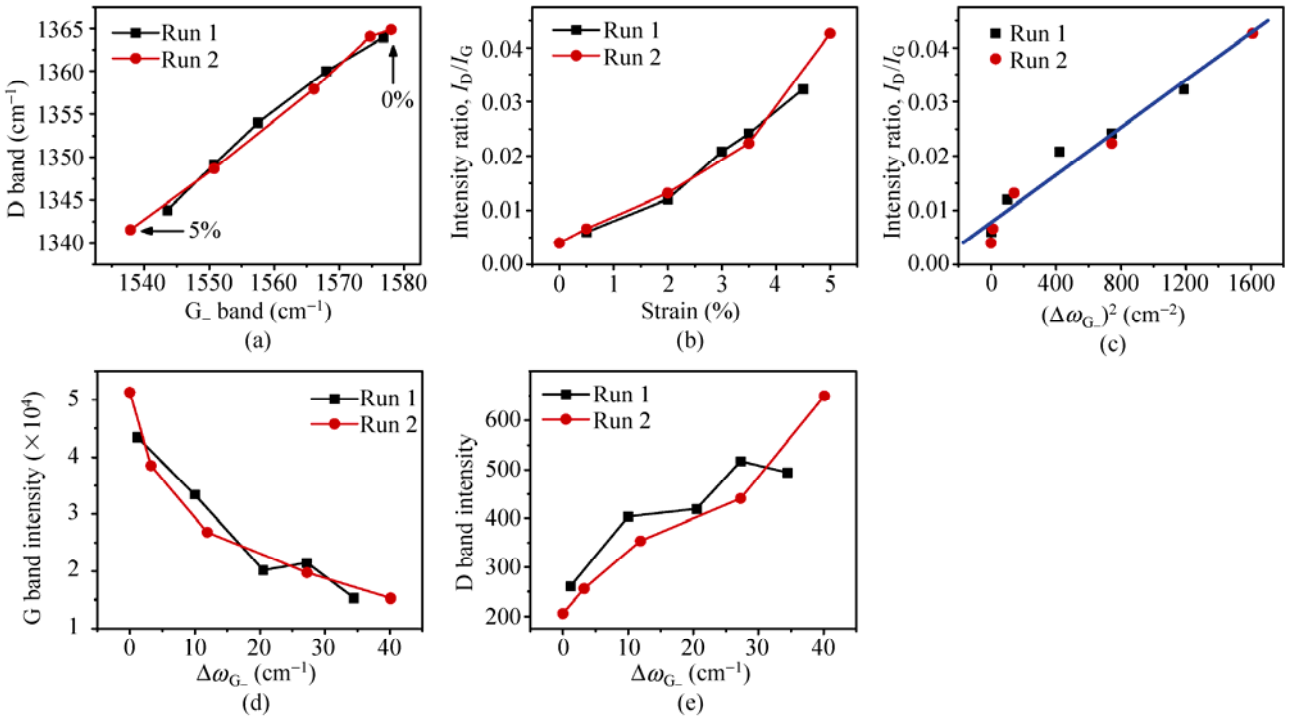

Figure 3 (a) D band Raman frequency plotted as a function of G_ band frequency. (b) and (c) Raman intensity of G and D band plotted as a function of the G_ band shift ($\Delta\omega_{G\_}$). (d) and (e) Intensity ratio of D to G band plotted as a function of applied strain and the square of the G_ band frequency, respectively

of uniaxial strain also break the symmetry of the lattice, and can result in relaxation of the selection rules. The intensity of the so-called defect-induced D band has been used to indicate the quality of carbon nanotubes for many years [10–12]. However, what we observe here are reversible changes in the D band intensity. This indicates that we are not actually creating permanent defects, but that the strain (5%) induces a lattice distortion large enough to distort the sp^2 symmetry, making the D band observable. The diagram in Fig. 4 shows the double resonance (DR) process where the phonon wavevector connects the points *A* and *B* in a hexagonal Brillouin zone (BZ) of a non-strained hexagonal lattice (here we are only considering the dominant inner DR process) [25]. A defect is needed to bring back the electron from *B* to *A*.

Let us now consider a graphene layer, with a uniaxial strain applied along either the zig-zag or armchair direction. The origin of the D band is a double resonance intervalley process that, in hexagonal lattices, requires a finite momentum, which is represented by

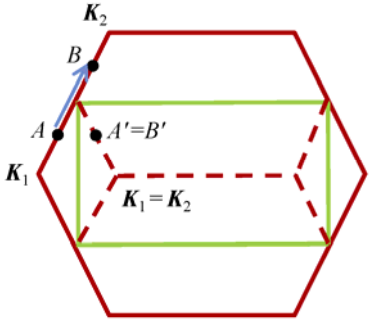

Figure 4 Double resonance process in the hexagonal (in red) and orthorhombic (in green) BZ. The orthorhombic BZ is generated by folding the hexagonal BZ along the green lines

the blue arrow connecting the *A* and *B* points in Fig. 4. This distortion will decrease the lattice symmetry from hexagonal to orthorhombic, the orthorhombic unit cell being twice that of the hexagonal one. The orthorhombic BZ zone can be generated by folding the hexagonal BZ, as shown in Fig. 4. When the hexagonal BZ is folded into the orthorhombic BZ under strain, however, the points *A* and *B* are folded onto the same point in the orthorhombic zone of a strained hexagonal

lattice. In this case, no defect is needed to activate the D band phonon. Symmetry lowering from a hexagonal to an orthorhombic lattice can be achieved under large axial strain. This argument is strictly valid only for a graphene layer, since carbon nanotubes are a one-dimensional system, with symmetries that depends on their chiral angle. However, since many nanotubes properties can be obtained from the graphene electronic dispersion, by considering the cutting lines in the extended Brillouin zone, we expect that the strain-induced symmetry lowering will also activate the D band for carbon nanotubes. There have been several reports of Raman spectroscopy of graphene under strain, none of which report any change in the D band Raman intensity under strain [26–30]. Therefore, it is likely that our observation of the D band mode under strain may not arise from the distortion of the Brillouin zone, but rather to the locally induced deformations, as described below.

Another possibility is that the nanotubes are twisted in a bundle, and as strain is applied, local deformations (i.e. pinching) are created along the length of the resonant nanotube that subside after releasing the tension. Such local deformations have been created using an AFM tip, resulting in reversible changes in the conductance by up to two orders of magnitude. According to molecular dynamic simulations, the significant change in conductance was attributed to a reversible transition from sp^2 to sp^3 bond configurations in the local bending region [31, 32].

Figure 5(a) shows the Raman spectra of an ultra-long SWCNTs bundle strained on a PDMS substrate. At zero strain, there are two sharp G bands (G1 and G2), indicating that the bundle consists of two Raman resonant nanotubes (NT1 and NT2). Again, a small D band can be seen in this bundle at 0% strain. As the strain is increased, the D band downshifts in frequency and grows in intensity. Figures 5(b) and 5(c) show reversible changes in the Raman frequency up to 8% strain, for the D and G2 bands, respectively. However,

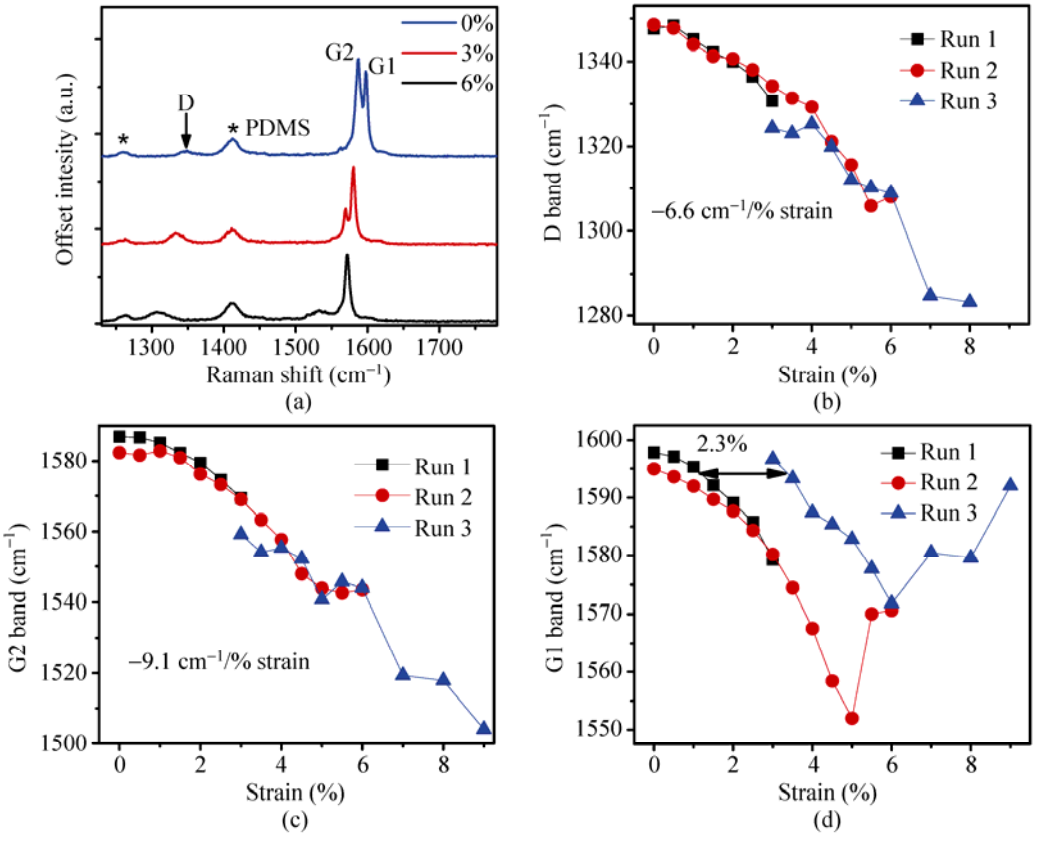

Figure 5 (a) Raman spectra of on-substrate carbon nanotubes at strains of 0, 3, and 6%. (b)–(d) D, G2, and G1 band frequencies plotted as a function of applied strain. Run 1 starts from 0% strain and is increased to 3% strain. Then, the strain is released to 0% and increased to 6% for run 2. Run 3 starts from 3%, and is increased up to 9%

irreversible changes of the G1 band frequency were observed after 5% strain. Beyond 5%, the G1 band upshifts from 1552 to 1571 cm^{-1}, due to slippage between NT1 and the underlying substrate, as shown in Fig. 5(d). Hysteresis plays an important role in these measurements, by indicating the occurrence of slippage. There is no hysteresis in the Raman downshift of the D and G2 bands, as shown in Figs. 5(b) and 5(c). The hysteresis in the G1 band frequency, however, indicates slippage at 5% strain. AFM has been used to reveal the buckling of strain-relaxed nanotubes [33]. The Raman frequency of the D band remains downshifted after 5% strain, as with the G2 band, indicating that the D band origins from NT2 only. Due to the strong dependence on chirality, strain-induced G band downshifts span a wide range from –6.2 to –23.6 cm^{-1}/% strain [5, 34–36]. Before slippage, the G band downshifted at a rate of approximately –8 to –9 cm^{-1}/% strain, which lies within the range of previously reported values.

The D band frequency can be plotted as a linear function of the G2 band frequency, as shown in Fig. 6(a), indicating that these two modes originate from the same SWCNT. The intensity ratio I_D/I_{G2} is plotted as a function of strain in Fig. 6(b) and varies from 0.01 to 1.34 with a quadratic dependence similar to that shown in Fig. 3(b). The G band downshift provides a more reliable measure of the C–C bond elongation, and yields a more clear plot of the intensity ratio as a function of the square of the G2 band downshift ($\Delta\omega_{G2}^2$), as shown in Fig. 6(c). The quadratic dependence shown here is consistent with the data shown in Fig. 3(c). Again, we observe that the G2 band Raman intensity decreases inversely with $\Delta\omega_{G2}$ and the D band intensity increases proportional to $\Delta\omega_{G2}$, as shown in Figs. 6(d) and 6(e). All samples measured in this work show a reversible increase in the D band linewidth with strain, as plotted in Figs. S-1(a) and S-1(b) in the Electronic Supplementary Material (ESM). Interestingly, the linewidths observed in the suspended sample (Fig. 2) are around 6 cm^{-1}. This is considerably narrower than previous reports of D band linewidths, which are typically in the range of 10–35 cm^{-1} [37]. Recently, narrow peaks (8 cm^{-1}) have been observed in the Raman spectra of bilayer graphene, and attributed to symmetry breaking by Moiré patterns of twisted

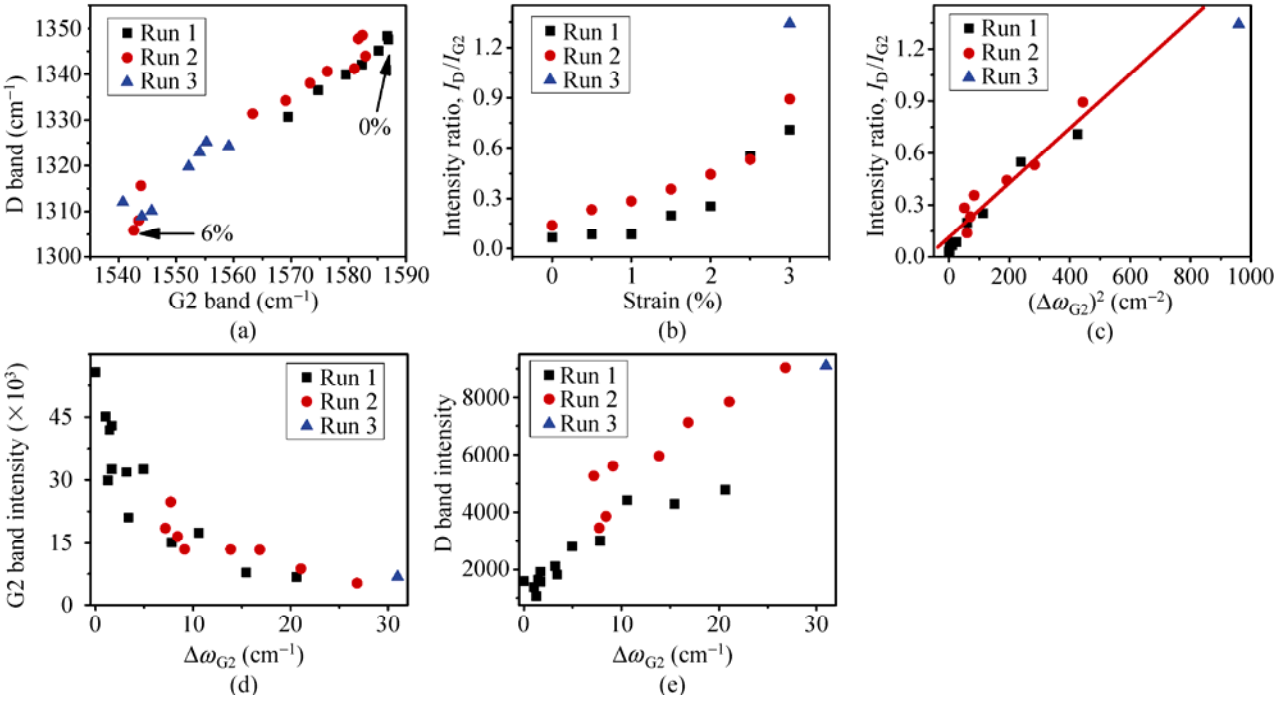

Figure 6 (a) D band Raman frequency plotted as a function of G2 band frequency. (b) and (c) Raman intensity of G2 and D band plotted as a function of the G2 band shift ($\Delta\omega_{G2}$). (d) and (e) Intensity ratio of D to G2 band plotted as a function of applied strain and the square of the G2 band shift, respectively

layers of graphene, which activates a double resonance process [38].

Figure 7 shows the raw Raman spectra of the nanotube shown in Figs. 5 and 6 taken at various degrees of strain. At strains of 2.5% and 4%, the G2 band intensity decreases significantly with strain. The G1 and G2 bands overlap at strains between 4 and 5%, making it difficult to obtain reliable intensity data in this range of strain. As we can see in the spectrum of Fig. 7(c) taken at 5.5% strain, the G1 and G2 bands become well separated after the slippage of NT1 at 5% strain. However, for strains higher than 7%, we begin to observe an additional peak between 1500 and 1600 cm^{-1}, as indicated by the arrow in the Fig. 7(d), which may be due to other nanotubes within the bundle shifting onto resonance with the laser energy or to other non-Raman active modes becoming observable due to the lowering of the lattice symmetry under stain [39]. The D band downshifts from 1348 to 1282 cm^{-1} before it merges with the PDMS peak at 1260 cm^{-1}. After relaxing the strain, there was no detectable increase in I_D/I_{G2} of this bundle from its original intensity ratio, as shown in Fig. 6(b). We exclude the possibility of breaking C–C bonds at high strains and reconstruction of bonds when strain is released since this process would require a large amount of energy and the experiments were carried at room temperature [40]. The strain-induced D band requires a detailed theoretical calculation to provide a deeper understanding.

In conclusion, we observe an increase in the D to G mode Raman intensity ratio (I_D/I_G) in carbon nanotubes under the application of uniaxial strain. A 100-fold increase in the I_D/I_G ratio is observed at strains of 5%. However, all changes in the Raman spectra are reversible with strain, indicating that no permanent defects are formed in the lattice under the applied strains. Instead, the change in I_D/I_G ratio arises from a lowering of the symmetry of the lattice under these large strains.

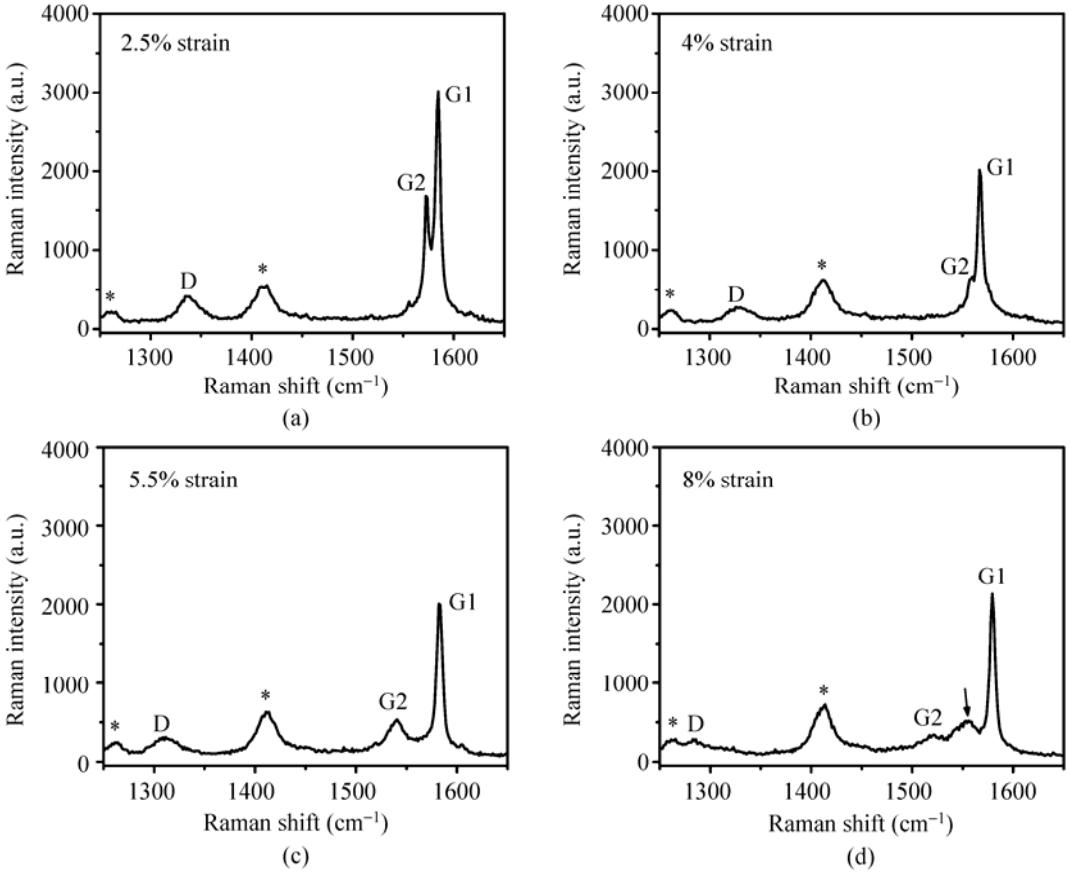

Figure 7 Raman spectra of the on-substrate carbon nanotubes shown in Figs. 5 and 6 under various degrees of strain. The * symbol indicates peaks originating from the underlying PDMS substrate

Acknowledgements

This research was supported in part by Department of Energy (DOE) Award (No. DE-FG02-07ER46376) and Office of Naval Research (ONR) Award (No. N000141010511). The authors would like to thank Prof. Helio Chacham for helpful discussions.

Electronic Supplementary Material: Supplementary material (D band linewidth plotted as a function of strain for suspended and on-substrate carbon nanotubes and raw spectra of suspended and on-substrate CNTs at 5% strain) is available in the online version of this article at http://dx.doi.org/10.1007/s12274-012-0269-3.

References

[1] Sazonova, V.; Yalsh, Y.; Üstünel, H.; Roundy, D.; Arias, T. A.; McEuen, P. L. A tunable carbon nanotube electromechanical oscillator. *Nature* **2004**, *431*, 284–287.

[2] Chiu, H. -Y.; Hung, P.; Postma, H. W. C.; Bockrath, M. Atomic-scale mass sensing using carbon nanotube resonators. *Nano Lett.* **2008**, *8*, 4342–4346.

[3] Yakobson, B.; Smalley, R. Fullerene nanotubes: $C_{1,000,000}$ and beyond. *Am. Scientist* **1997**, *85*, 324–337.

[4] Pugno, N. M. On the strength of the carbon nanotube-based space elevator cable: From nanomechanics to megamechanics. *J. of Phys.: Condens Matter* **2006**, *18*, S1971–S1990.

[5] Chang, C.-C.; Hsu, I. K.; Aykol, M.; Hung, W.-H.; Chen, C.-C.; Cronin, S. B. A new lower limit for the ultimate breaking strain of carbon nanotubes. *ACS Nano* **2010**, *4*, 5095–5100.

[6] Zhang, R. F.; Wen, Q.; Qian, W. Z.; Su, D. S.; Zhang, Q.; Wei, F. Superstrong ultralong carbon nanotubes for mechanical energy storage. *Adv. Mater.* **2011**, *23*, 3387–3391.

[7] Zhao, Q. Z.; Nardelli, M. B.; Bernholc, J. Ultimate strength of carbon nanotubes: A theoretical study. *Phys. Rev. B* **2002**, *65*, 144105.

[8] Dumitrica, T.; Hua, M.; Yakobson, B. I. Symmetry-, time-, and temperature-dependent strength of carbon nanotubes. *Proc. Natl. Acad. Sci. U. S. A.* **2006**, *103*, 6105–6109.

[9] Matthews, M. J.; Pimenta, M. A.; Dresselhaus, G.; Dresselhaus, M. S.; Endo, M. Origin of dispersive effects of the Raman D band in carbon materials. *Phys. Rev. B* **1999**, *59*, R6585–R6588.

[10] Dresselhaus, M. S.; Dresselhaus, G.; Saito, R.; Jorio, A. Raman spectroscopy of carbon nanotubes. *Phys. Rep.* **2005**, *409*, 47–99.

[11] Dresselhaus, M. S.; Jorio, A.; Hofmann, M.; Dresselhaus, G.; Saito, R. Perspectives on carbon nanotubes and graphene Raman spectroscopy. *Nano Lett.* **2010**, *10*, 751–758.

[12] Hulman, M.; Skákalová, V.; Roth, S.; Kuzmany, H. Raman spectroscopy of single-wall carbon nanotubes and graphite irradiated by gamma rays. *J. Appl. Phys.* **2005**, *98*, 024311.

[13] Lucchese, M. M.; Stavale, F.; Ferreira, E. H. M.; Vilani, C.; Moutinho, M. V. O.; Capaz, R. B.; Achete, C. A.; Jorio, A. Quantifying ion-induced defects and Raman relaxation length in graphene. *Carbon* **2010**, *48*, 1592–1597.

[14] Cançado, L. G.; Jorio, A.; Ferreira, E. H. M.; Stavale, F.; Achete, C. A.; Capaz, R. B.; Moutinho, M. V. O.; Lombardo, A.; Kulmala, T. S.; Ferrari, A. C. Quantifying defects in graphene via Raman spectroscopy at different excitation energies. *Nano Lett.* **2011**, *11*, 3190–3196.

[15] Cronin, S. B.; Swan, A. K.; Ünlü, M. S.; Goldberg, B. B.; Dresselhaus, M. S.; Tinkham, M. Measuring the uniaxial strain of individual single-wall carbon nanotubes: Resonance Raman spectra of atomic-force-microscope modified single-wall nanotubes. *Phys. Rev. Lett.* **2004**, *93*, 167401.

[16] Kumar, R.; Aykol, M.; Ryu, K.; Zhou, C. W.; Cronin, S. B. Top-down lithographic method for inducing strain in carbon nanotubes. *J. Appl. Phys.* **2009**, *106*, 014306.

[17] Cronin, S. B.; Swan, A. K.; Ünlü, M. S.; Goldberg, B. B.; Dresselhaus, M. S.; Tinkham, M. Resonant Raman spectroscopy of individual metallic and semiconducting single-wall carbon nanotubes under uniaxial strain. *Phys. Rev. B* **2005**, *72*, 035425.

[18] Frogley, M. D.; Zhao, Q.; Wagner, H. D. Polarized resonance Raman spectroscopy of single-wall carbon nanotubes within a polymer under strain. *Phys. Rev. B* **2002**, *65*, 113413.

[19] Lucas, M.; Young, R. J. Effect of uniaxial strain deformation upon the Raman radial breathing modes of single-wall carbon nanotubes in composites. *Phys. Rev. B* **2004**, *69*, 085405.

[20] Kumar, R.; Cronin, S. B. Raman scattering of carbon nanotube bundles under axial strain and strain-induced debundling. *Phys. Rev. B* **2007**, *75*, 155421.

[21] Son, H.; Samsonidze, G. G.; Kong, J.; Zhang, Y. Y.; Duan, X. J.; Zhang, J.; Liu, Z. F.; Dresselhaus, M. S. Strain and friction induced by van der Waals interaction in individual single walled carbon nanotubes. *Appl. Phys. Lett.* **2007**, *90*, 253113.

[22] Huang, M.; Wu, Y.; Chandra, B.; Yan, H.; Shan, Y.; Heinz, T. F.; Hone, J. Direct measurement of strain-induced changes in the band structure of carbon nanotubes. *Phys. Rev. Lett.* **2008**, *100*, 136803.

[23] Jorio, A.; Souza Filho, A. G.; Dresselhaus, G.; Dresselhaus, M. S.; Saito, R.; Hafner, J. H.; Lieber, C. M.; Matinaga, F. M.; Dantas, M. S. S.; Pimenta, M. A. Joint density of electronic states for one isolated single-wall carbon nanotube studied by resonant Raman scattering. *Phys. Rev. B* **2001**, *63*, 245416.

[24] Cao, J.; Wang, Q.; Dai, H. J. Electromechanical properties of metallic, quasimetallic, and semiconducting carbon nanotubes under stretching. *Phys. Rev. Lett.* **2003**, *90*, 157601.

[25] Venezuela, P.; Lazzeri, M.; Mauri, F. Theory of double-resonant Raman spectra in graphene: Intensity and line shape of defect-induced and two-phonon bands. *Phys. Rev. B* **2011**, *84*, 035433.

[26] Ni, Z. H.; Yu, T.; Lu, Y. H.; Wang, Y. Y.; Feng, Y. P.; Shen, Z. X. Uniaxial strain on graphene: Raman spectroscopy study and band-gap opening. *ACS Nano* **2008**, *2*, 2301–2305.

[27] Mohiuddin, T. M. G.; Lombardo, A.; Nair, R. R.; Bonetti, A.; Savini, G.; Jalil, R.; Bonini, N.; Basko, D. M.; Galiotis, C.; Marzari, N.; Novoselov, K. S.; Geim, A. K.; Ferrari, A. C. Uniaxial strain in graphene by Raman spectroscopy: G peak splitting, Grüneisen parameters, and sample orientation. *Phys. Rev. B* **2009**, *79*, 205433.

[28] Huang, M. Y.; Yan, H. G.; Chen, C. Y.; Song, D. H.; Heinz, T. F.; Hone, J. Phonon softening and crystallographic orientation of strained graphene studied by Raman spectroscopy. *Proc. Natl. Acad. Sci. U. S. A.* **2009**, *106*, 7304–7308.

[29] Frank, O.; Mohr, M.; Maultzsch, J.; Thomsen, C.; Riaz, I.; Jalil, R.; Novoselov, K. S.; Tsoukleri, G.; Parthenios, J.; Papagelis, K.; Kavan, L.; Galiotis, C. Raman 2D-band splitting in graphene: Theory and experiment. *ACS Nano* **2011**, *5*, 2231–2239.

[30] Huang, M.; Yan, H.; Heinz, T. F.; Hone, J. Probing strain-induced electronic structure change in graphene by Raman spectroscopy. *Nano Lett.* **2010**, *10*, 4074–4079.

[31] Liu, L.; Jayanthi, C. S.; Tang, M. J.; Wu, S. Y.; Tombler, T. W.; Zhou, C. W.; Alexseyev, L.; Kong, J.; Dai, H. J. Controllable reversibility of an sp^2 to sp^3 transition of a single wall nanotube under the manipulation of an AFM tip: A nanoscale electromechanical switch? *Phys. Rev. Lett.* **2000**, *84*, 4950–4953.

[32] Tombler, T. W.; Zhou, C. W.; Alexseyev, L.; Kong, J.; Dai, H. J.; Liu, L.; Jayanthi, C. S.; Tang, M. J.; Wu, S.-Y. Reversible electromechanical characteristics of carbon nanotubes under local-probe manipulation. *Nature* **2000**, *405*, 769–772.

[33] Maune, H.; Bockrath, M. Elastomeric carbon nanotube circuits for local strain sensing. *Appl. Phys. Lett.* **2006**, *89*, 173131.

[34] Yang, W.; Wang, R.-Z.; Yan, H. Strain-induced Raman-mode shift in single-wall carbon nanotubes: Calculation of force constants from molecular-dynamics simulations. *Phys. Rev. B* **2008**, *77*, 195440.

[35] Wu, G.; Zhou, J.; Dong, J. M. Raman modes of the deformed single-wall carbon nanotubes. *Phys. Rev. B* **2005**, *72*, 115411.

[36] Gao, B.; Jiang, L.; Ling, X.; Zhang, J. F.; Liu, Z. Chirality-dependent Raman frequency variation of single-walled carbon nanotubes under uniaxial strain. *J. Phys. Chem. C* **2008**, *112*, 20123–20125.

[37] Jorio, A.; Fantini, C.; Dantas, M. S. S.; Pimenta, M. A.; Souza Filho, A. G.; Samsonidze, G. G.; Brar, V. W.; Dresselhaus, G.; Dresselhaus, M. S.; Swan, A. K.; Ünlü, M. S.; Goldberg, B. B.; Saito, R. Linewidth of the Raman features of individual single-wall carbon nanotubes. *Phys. Rev. B* **2002**, *66*, 115411.

[38] Righi, A.; Costa, S. D.; Chacham, H.; Fantini, C.; Venezuela, P.; Magnuson, C.; Colombo, L.; Bacsa, W. S.; Ruoff, R. S.; Pimenta, M. A. Graphene Moiré patterns observed by umklapp double-resonance Raman scattering. *Phys. Rev. B* **2011**, *84*, 241409.

[39] Araujo, P. T.; Barbosa Neto, N. M.; Chacham, H.; Carara, S. S.; Soares, J. S.; Souza, A. D.; Cançado, L. G.; de Oliveira, A. B.; Batista, R. J. C.; Joselevich, E.; Dresselhaus, M. S.; Jorio, A. *In situ* atomic force microscopy tip-induced deformations and Raman spectroscopy characterization of single-wall carbon nanotubes. *Nano Lett.* **2012**, *12*, 4110–4116.

[40] Stone, A. J.; Wales, D. J. Theoretical studies of icosahedral C_{60} and some related species. Chem. Phys. Lett. **1986**, *128*, 501–503.